ASWAN HEART CENTRE
SCIENCE & PRACTICE SERIES
A Qatar Foundation Academic Journal

OPEN ACCESS

Review article

Computational biomechanics of the aortic root

Ryo Torii[1,2,5,*], Xiao Yun Xu[5], Ismail El-Hamamsy[4], Raad Mohiaddin[3] and Magdi H. Yacoub[1,2]

[1]Qatar Cardiovascular Research Center, Doha, Qatar
[2]Harefield Heart Science Centre, Imperial College London, Harefield, UK
[3]Cardiovascular Magnetic Resonance Unit, Royal Brompton Hospital and Imperial College London, London, UK
[4]Department of Cardiac Surgery, Montreal Heart Institute, Montreal, Canada
[5]Department of Chemical Engineering, Imperial College London, London, UK
*Email: r.torii@imperial.ac.uk

INTRODUCTION

The aortic valve and root perform extremely sophisticated functions that are critically dependent on their topology as well as the structure of their component parts at tissue, cellular and molecular levels [1]. Each of these components is capable of changing its size and shape during different phases of the cardiac cycle [2–7] (Fig. 1). Computational biomechanics offers unique opportunities to study many of these functions in humans. Rapid progress in this field has resulted in the accumulation of a large amount of knowledge relating to this topic. We here describe the application of biomechanics to the study of the aortic root in health and disease as well as following different types of valve preserving and aortic root replacement using biological valves.

Biomechanics

This includes study of the dynamics of the aortic wall as well as defining spatio-temporal characteristics of flow in the aortic root, both of which are thought to influence cardiac function, coronary flow [8] and distribution of blood to vital organs [1]. Using computational analysis along with sophisticated medical imaging techniques, physiological parameters that are inherently not possible or extremely difficult to measure directly *in vivo* can be quantified. These parameters include stress distribution, either in terms of shear stress exerted by the blood flow on the endothelium or of tensile stress in the tissue such as the arterial wall.

METHODOLOGY

Computational biomechanics for *in vivo* characterisation of human (patho)physiology is based on detailed medical images such as high-definition multi-slice CT and cardiovascular MRI. The imaging data are mostly used to construct an anatomical model of an organ in which physiological parameters, e.g. endothelial shear stress (ESS) and wall tensile stress, are calculated computationally. A typical procedure for subject-specific blood flow modelling is illustrated in Fig. 2.

Imaging and anatomical model reconstruction

Cardiovascular Magnetic Resonance Imaging (CMR) of aortic anatomy uses high-resolution cardiac and respiratory gated 3D steady-state in free precession (SSFP) acquired in transversal plane and multiple 2D fast spin-echo in selective planes. Breath-hold Cine SSFP was used to produce dynamic images of the aortic root and aortic valve motion and of the aortic wall and the left ventricle. In addition CMR phase-contrast technique using gradient echo sequence was used to measure blood flow and blood flow velocity at aortic valve level or any other desirable plane transecting the aorta. These values are typically acquired using a common 1.5/3.0 Tesla scanner. Electrocardiogram-gated multi-slice CT can also be used to obtain anatomical information, including its dynamic aspect. In general, CT has higher in-plane resolution than CMR, and hence it was preferred for anatomical information to be used in computational biomechanics, but an iodinated contrast agent is required, and X-ray radiation is an important issue. However, recent developments in CMR imaging—better motion compensation and imaging sequences design—allow high-resolution anatomical and dynamic images to be obtained for computational modelling without X-ray radiation or the need for

DOI: http://dx.doi.org/10.5339/ahcsps.2011.16
Published: 30 December 2011

QSCIENCE.com
Member of Qatar Foundation

Cite this article as: Torii R, Xu XY, El-Hamamsy I, Mohiaddin R, Yacoub MH. Computational biomechanics of the aortic root, *Aswan Heart Centre Science & Practice Series* 2011:16
doi: http://dx.doi.org/10.5339/ahcsps.2011.16

contrast agent injection. This technique also provides simultaneous assessment of anatomy as well as detailed information on blood flow and cardiac function. Subject-specific 3D anatomical models (the aorta in Fig. 2) can be reconstructed from these medical images by segmenting the scanned volume based on image intensities.

The second step is to mesh the geometry. This is to create fine grids in the volume enclosed by the reconstructed 3D surface. The governing equations, for example the Navier–Stokes equations for blood flow, are solved on this mesh, and variables such as blood velocity and pressure are calculated at each grid point. There are various mesh types available: tetrahedral, prism, pyramid and

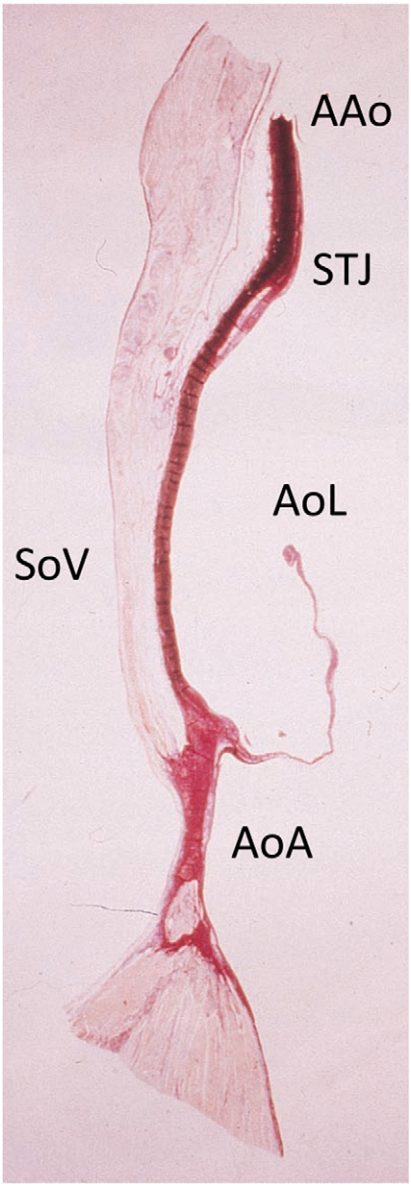

Figure. 1 Longitudinal section of the normal aortic valve. The aortic annulus (AoA) is a crown-shaped three-pointed structure, in spite of its name, which implies a ring. The annulus is a definite fibrous structure that, apart from giving origin to the aortic leaflets (AoL), is firmly attached to the media of aortic sinuses distally, while proximally it is attached to the muscular and the membranous septa anteriorly, the fibrous trigones laterally, and the subaortic curtain posteriorly. The latter three structures, together with the annulus, form part of the fibrous framework of the heart. The sinuses of Valsava (SoV) constitute three almost symmetrical bulges in the aortic root extending from the aortic annulus to the sinotubular junction (STJ), where the root joins the ascending aorta (AAo). The media of the aortic sinuses diminish progressively in thickness from the level of the sinotubular junction towards the annulus, where it is firmly fixed.

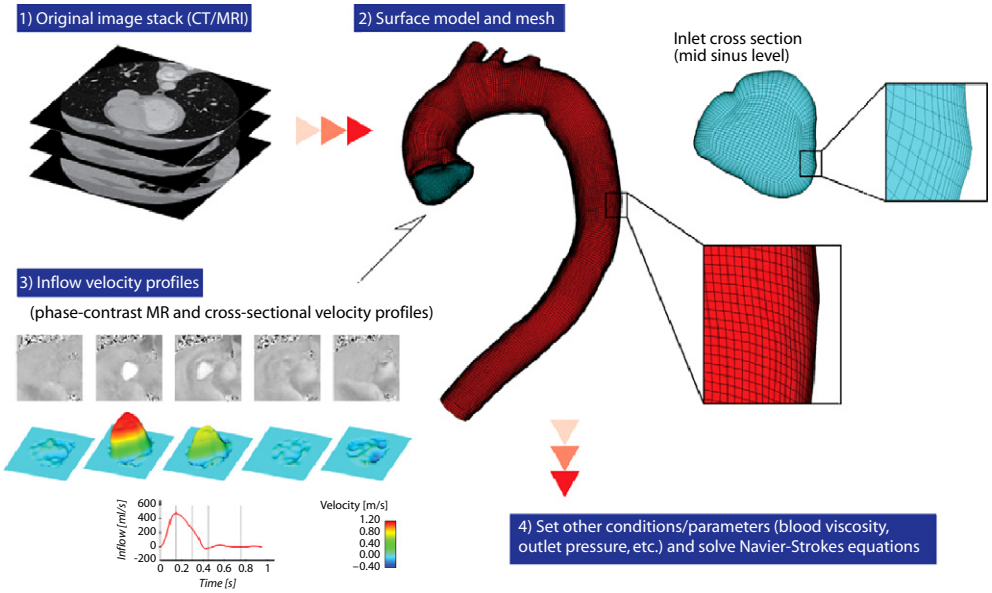

Figure. 2 Typical procedure for subject-specific blood flow computation. (A) acquisation of clinical images, (B) image segmentation and mesh generation, (C) applying boundary conditions (inflow velocity profiles at mid-sinus level in this example) and (D) setting physical properties such as blood density and viscosity, before solving the equations for fluid motion, i.e. Navier–Stokes equations.

hexahedral (brick) shapes are commonly used in 3D computations. Because spatial gradients of variables in the governing equations are calculated based on the mesh, it is essential that the mesh is fine enough to resolve important features of the physical phenomena concerned. For example, blood flow velocity at the vessel wall is close to zero but it may change rapidly with the distance from the wall. Hence a fine mesh is required to capture the detailed velocity profile near the vessel wall.

Assumptions and conditions

Once a computational mesh is ready, physical conditions of the problem need to be specified. These include, for blood flow simulations, blood density and viscosity, as well as boundary conditions such as velocity at the inlet. For solid mechanics simulations, vessel wall density and elasticity (stress–strain relationship), as well as blood pressure and constraint conditions, are typically needed. At this point, one needs to consider assumptions and approximations carefully with respect to the aim of computation and key physics involved in the problem. For example, spatio-temporal evolution of the flow velocity through the aortic valve shows a highly complicated non-uniform pattern, as in Fig. 2. Recent advances in imaging techniques have enabled realistic inflow conditions to be applied by use of a velocity mapping technique as demonstrated in Fig. 2. However, in most studies these complicated inflow patterns were modelled using simplified profiles, such as the Womersley velocity profile [9] or a uniform profile, since access to subject-specific flow data is not always available. It has been shown that downstream flow patterns calculated with a simplified inflow profile are different from those obtained with realistic inflow conditions. For example, comparisons of computed aortic flow patterns and resulting ESS between spatially-uniform and parabolic inlet velocity profiles as well as a more realistic model incorporating the left ventricle showed a maximum of 4-fold difference in ESS in the ascending aorta, ranging from 0.5 to 2 Pa, although the difference was negligible in the middle of the aortic arch [10]. Computations are faster when the physics incorporated is simpler, hence it is important to strike a balance between model complexity and computational efficiency. A preferred approach is to keep the model simple while containing essential details, thus it is crucial to validate the computational model. The anatomical model, model assumptions and boundary conditions are then fed to a validated computational fluid or solid mechanics solver where an appropriate set of equations (e.g. Navier–Stokes equations for blood flow) are solved numerically, and relevant variables are calculated, which can be visualised as shown in Fig. 3.

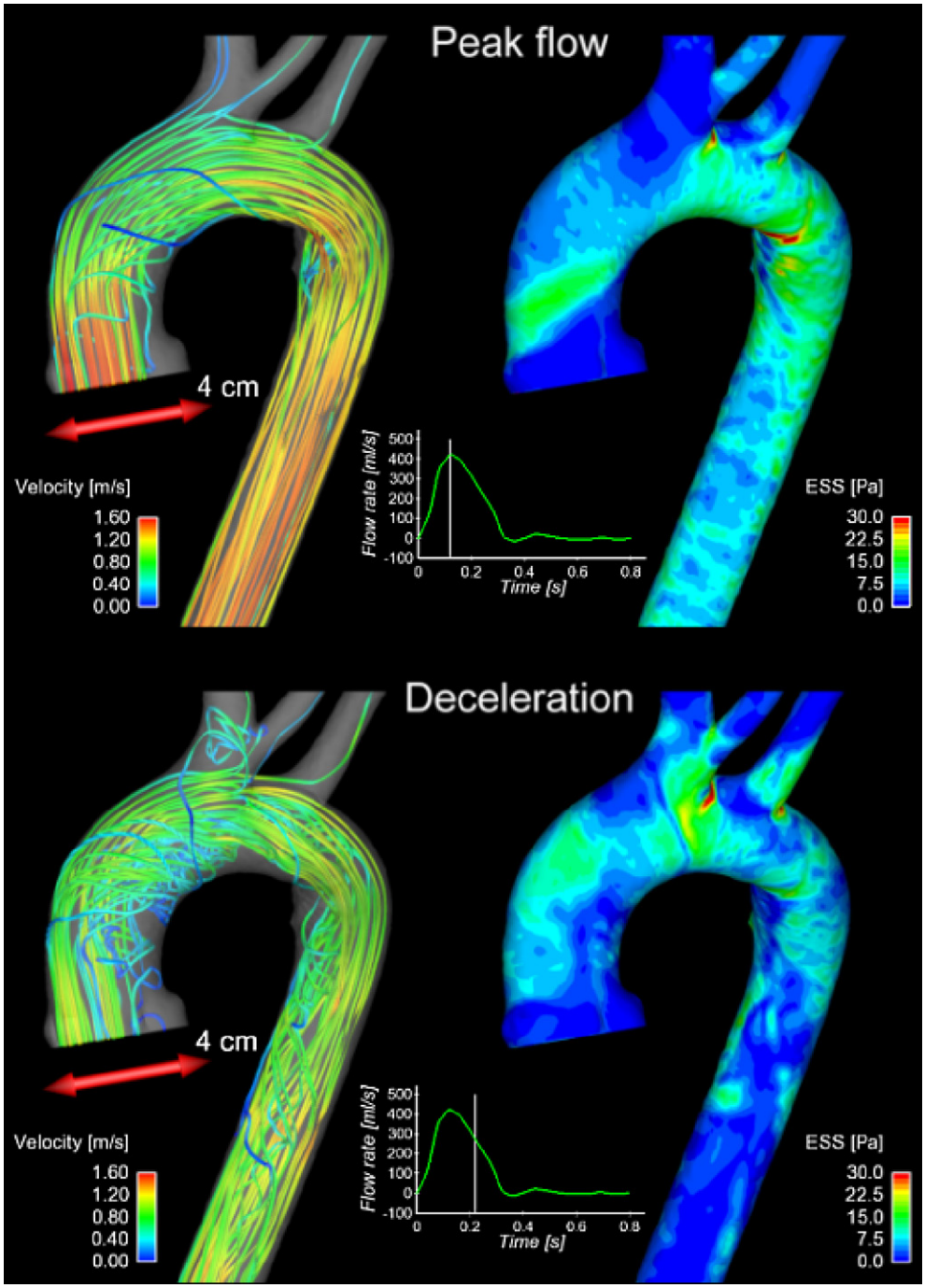

Figure. 3 Example of blood flow simulation results. Streamline representation of blood flow patterns (left) and ESS maps (right) at two different phases in a cardiac cycle. At peak flow, streamlines are straight through the aorta whereas they show strongly swirling patterns in the deceleration phase.

Validation

Because the use of model assumptions is inevitable in computational simulations, it is important to test their reliability, which includes evaluation of the reproducibility and accuracy of the method, and vigorous validation of the numerical solutions. Reproducibility of a subject-specific blood flow computation was tested with 3D ultrasound-based [11] and MRI-based [12] anatomical models and a good reproducibility with eight per cent of ESS variability for multiple trials shown. Numerous validation attempts have been made, including comparisons between computational results and measurements made on *in vitro* physical models [13,14]. Furthermore, recent advances in imaging

techniques enabled comparisons with *in vivo* data, as demonstrated by comparisons between computational predictions and MR measurements, reported in [15,16]. A good agreement between computational and experimental results would provide some confidence in the reliability of the computational models used. Due to the complexity of physiological systems, it is unlikely that a single computational model is valid universally. Hence, careful tests need to be performed for an individual application in order to understand potential drawbacks and gain confidence in the method.

APPLICATIONS

In health

Blood flow

Because of evidences linking ESS and pathophysiology such as atherosclerosis [17] and aneurysm [1], computational fluid dynamics (CFD) has been extensively applied in normal human circulatory systems to quantify ESS in order to understand normal haemodynamics and initial stage of disease [18]. The aortic flow, ejected through the aortic valve by the left ventricular contraction, is well known to have a spiral pattern that is associated with the anatomy of the aorta [19], vortical flow in the left ventricle [20,21] and dynamics of the aortic root [22]. This spiral flow characteristic was suggested to help blood flow progression in the aorta by minimising turbulence and associated energy loss [19]. It has indeed been proposed to quantify the spiral pattern with a helicity parameter in order to assess the normality of aortic flow [23]. One of the major determinants in aortic flow, the aortic root anatomy, varies considerably even in normal cases, from the left ventricular outflow tract with elliptic cross-section [24], through the sinuses to ascending aorta [25]. And with dynamism of these components, aortic flow exhibits complicated patterns in comparison to other parts of the cardiovascular system.

Three-dimensional, computational analyses of flow in the aorta were initially attempted on the aorto-iliac bifurcation [26] and abdominal aortic aneurysm [27] because of geometrical simplicity, followed by those on descending [28] and ascending aortas [29–32]. These studies aimed to understand fundamental flow and resulting ESS patterns in the aorta. Among them was the investigation, by Black et al., of the effect of aortic arch anatomy on flow patterns using varying hypothetical aortic anatomy: a good example of applying CFD to aortic flow problems [31]. Recent studies were carried out with a focus on more clinically-relevant output and in relation to biological factors, which will be discussed later.

Aortic wall mechanics

Stress and strain are also known to affect vascular biology, particularly those factors related to vascular tone [33] and inflammation [34], which in turn would affect stress levels [35]. Hence quantifying stress levels in the aortic wall is important for us to understand tissue damage and remodelling for which studying normal subjects is a good starting point. The simplest but effective way of estimating stress is to use Laplace's law that relates circumferential (hoop) stress in the vessel wall to its radius, thickness and internal pressure ($\tau = Pr/h$)[1]. This equation was first applied to *in vivo* observation of myocardium in early 70s by Role and co-workers [36] and has been used as an effective measure since. In real *in vivo* circumstances, pressure varies locally and it is difficult to obtain the local radius accurately, because real arterial anatomy is far more complicated than a straight cylinder. A regional and more detailed distribution of stress can be given through its relationship with local strain, using a constitutive relation. Constitutive relationships can be as simple as linear elastic, i.e. stress $T = E\varepsilon$, where E is elastic (Young's) modulus and ε is strain. An early example of local stress quantification using a linear elastic constitutive relationship can be found in Clark et al., combining experimental observation on aortic valve with numerical modelling [37]. However, since it is well known that the arterial wall is a layered, fibre-reinforced structure of inhomogeneous compositions, which exhibits non-linear stress–strain relationship [1], the constitutive equation is expected to be more complicated, such as the one proposed by Raghavan et al. for abdominal aortic aneurysm tissue considering material nonlinearity [38], or the one by Gasser et al. including material nonlinearity, anisotropy and fibre orientations [39]. Using a constitutive equation, one can calculate tissue tensile stress from a known (measured or computed)

[1] P: inner pressure, r: vessel radius, h: vessel wall thickness

strain field. Finite element computational modelling has been extensively used to acquire local/regional tissue strain *in vivo*, as well as other image-based strain calculations such as ultrasound palpography and tagged MR. There is a substantial body of literature on computational analyses of deformation, strain and stress on arterial walls. In this approach, spatial resolution in the calculations (grid density) can be higher than available imaging techniques.

Interaction between blood flow and arterial wall structure

The aortic root changes its size and shape during different phases of the cardiac cycle in interaction with blood flow and cardiac motion [2–5,7]. A combined MR and CFD study [22] demonstrated that the spiral aortic flow pattern is largely determined by the cardiac-induced motion of the aortic root. This suggests, as also pointed out by Lansac et al. in their aortic root dynamics study [4], that substitution of a prosthetic graft for the aortic root could significantly alter the nature of aortic flow by restricting its dynamics and mobility.

Aortic root dynamics, as part of the Windkessel effect, contributes to high diastolic pressure difference between the sinus and the coronary circulation, which is a major driver of the diastolic-dominant coronary flow, in conjunction with myocardial relaxation [8,40]. It also affects coronary ostium dynamics as observed in a time-resolved multislice CT study [41]. It was reported that the entrance flow profile to the coronary ostia contributes significantly to the patterns of ESS in the proximal end of the artery [42]. The proximal segment of the coronary arteries is more prone to atherosclerosis and, based on the flow-mediated atherogenesis hypothesis, the entrance flow profile could play an important role in understanding coronary atherosclerosis. Additionally, since coronary arterial motion alters the oscillatory nature of its ESS [43,44], the coronary ostium motion pattern may also contribute to the determination of coronary flow patterns and thereby affect atherogenesis.

The bulging shape of the sinus and jet flow through the valve causes retrograde recirculating flow in the sinus as depicted in a number of studies [19,45,46]. This recirculating flow is known to help the valve closure [47,48] and was thought to affect the coronary flow since the coronary ostia are located on the sinus wall. A recent computational study demonstrated an insignificant effect of sinus morphology and resulting flow patterns on coronary flow [49]. However, it has been shown that improvement of coronary flow following a root replacement procedure depends on the type of substitutes [50,51], hence further investigation is needed to elucidate the link between sinus morphology and coronary flow.

In disease

ESS, atherosclerosis and aneurysm

Because blood flow and the resulting shear stress on the endothelium are thought to contribute to the tissue regulation in arterial wall [17], abnormal flow patterns are speculated to play an important role in pathophysiology in the aorta such as aortic dilatation/aneurysm [1] and atherosclerosis [52] by triggering maladaptive tissue regulations.

Computationally-derived ESS and related parameters have been compared with pathophysiological indices such as intima-media thickness (IMT) in early atherosclerotic circumstance. Jackson et al. compared computed post-operative (baseline) ESS in femoral vein graft patients with IMT at approximately 10 months follow-up; IMT at follow-up correlated with low WSS at baseline [53]. Augst et al. conducted a similar study on the carotid bifurcation and showed that blood pressure and ESS correlate with IMT [54]. Another ESS related parameter often referred to in relation to atherosclerosis is the oscillatory shear index (OSI) representing change in direction of ESS vector. Ku and fellows calculated ESS and OSI from velocity measurement in a plexiglass model, and compared them with IMT in a human carotid bifurcation sample [55]. Low and oscillatory ESS was found to collocate with thickened wall, which is believed to be a precursor of atherosclerotic plaques [56], suggesting its significant role in atherogenesis. High ESS is also associated with atherosclerosis; an *in vivo* study by Gijsen et al. suggested that high ESS influences atherosclerotic plaque composition via elevated strain [57]. Studies including biological aspects provide more insights into the mechanism underlying the relationship. Cheng and co-workers demonstrated a role of low and oscillatory ESS on expression of chemokines involved in atherogenesis using a mouse model [58]. Tarbell and his team demonstrated in their *in vitro* experiments that the phase difference between ESS and strain stimuli on ECs (stress phase angle, SPA) regulates nitric oxide and endothelin-1 productions [59–62]. This

finding was used in their computational study on the carotid artery to understand atherogenic blood flow patterns [63].

In a study related to the aorta, it was reported that high ESS is linked with local MMP-9 activity [64]. Although this study by Krams et al. [64] was focused on atherosclerotic plaque, active MMP-9 is thought to play an important role in aneurysm formation through matrix degeneration [1] and hence ESS might also be an important player in aortic aneurysm. In another example, artificially-induced atherosclerotic lesion morphology was compared with CFD-based ESS level in the carotid artery of mice [52]. Likewise, Vincent et al. compared CFD-based ESS patterns with fatty deposition patterns in mice aorta and showed a good correlation between them [65]. The relationship between aortic flow and the aortic valve — the most important component determining aortic flow — will be discussed later. Influence of ESS on the vasoactivity could be even more complicated in the aortic root considering the regional variability in endothelial cell response, as reported by Deck et al. on the difference between the endothelial cells on the ventricular side and aortic side of the aortic valve [66].

Transvalvular "jet" flow

When blood passes through the aortic valve, the blood pressure drops at the valve orifice. This is because the valve orifice area is smaller than the left ventricular outflow tract and ascending aorta; velocity through the narrower valve orifice is higher owing to mass conservation, and the pressure there is lower following the energy conservation (Bernoulli's principle: $1/2\rho v^2 + p =$ constant, where ρ, v and p are blood density, velocity and pressure). With a normal aortic valve, the velocity at the valve orifice is not very high, approximately 1.0 m/s [67], and hence the pressure drop at the orifice is small (4 mmHg for 1.0 m/s peak velocity). Therefore, the pressure is able to recover in the aorta downstream to a level that is only a few mmHg lower than the left ventricular pressure, i.e. transvalvular pressure gradient (TPG) is very small. The pressure recovery is deteriorated (=high TPG owing to turbulence [68]) when the valve orifice area is small due to valve disorders such as aortic stenosis; AHA classified severe aortic stenosis as TPG > 40 mmHg or orifice area <1.0 cm^2 [69] which is 1/4 to 1/3 of the normal orifice area [70]. High TPG results in an increased left ventricular (LV) load, which may cause LV remodelling and hypertrophy [71,72]. Transvalvular pressure gradient is typically estimated using the modified Bernoulli's equation [73]: TPG $= 4v_{VC}^2$ ($v_{VC} =$ velocity at vena contracta in m/s and TPG is calculated in mmHg), which was derived from the original Bernoulli's equation, $\Delta p = 1/2\rho v^2$, by using normal blood density (1060 kg/m^3) and converting the unit from Pa to mmHg. Otto and co-workers have reported, by a prospective investigation of asymptomatic adult valvular aortic stenosis patients, that jet velocity (and hence TPG calculated in this way) can be a predictor of clinical outcomes (death or aortic valve surgery) [74]. Further derivation of such haemodynamic parameters include energy loss: $E_L = 4v_{VC}^2(1 - (EOA/A_A)^2)$ (EOA: effective (valve) orifice area and A_A: aortic cross-sectional area) [75], its indexed variable (energy loss index), and impedance for aortic valve and downstream vasculature (Z_{va}: valvulo-arterial impedance) [76]. Following its definition, energy loss is high for high velocity at the vena contracta, small EOA and large aortic cross section. This can be explained by the fact that high velocity at the vena contracta, typically caused by small EOA, is likely to yield highly disturbed turbulent flow in the aorta that entails higher energy loss. A large aortic cross section such as aneurismal dilatation means sudden expansion in the aorta from the vena contracta to its downstream, which is also a typical cause of disturbed flow. Those energy-loss-based parameters are correlated well with clinical events (death or aortic valve replacement) and LV dysfunction for patients with aortic stenosis [75] and used to categorise patients. A high velocity jet could cause high ESS on the aortic wall [77,78], which is linked to aneurysmal aortic dilatation [1,79]. Such a high velocity jet can also occur in aortic coarctation, not only in the downstream of stenosed valves. Computational studies on a thoracic aortic aneurysm with coarctation [15] and type-B aortic dissection [80] both showed a high-speed jet occurring at the aortic coarctation and highly turbulent flow in the downstream opening which is accompanied by high energy loss in the blood flow.

Bicuspid aortic valve

The jet flow through the valve is likely to occur in patients with a bicuspid aortic valve (BAV). Having more structural constriction, BAV cannot open as much as tricuspid aortic valve. A rapid jet through a BAV, its impact on the ascending aortic wall and the resulting high ESS are all thought to be important

factors in understanding dilated aorta in BAV patients in relation to the orientation of the valve [77,82–85] (Fig. 5). Quantification of flow and haemodynamic wall shear stress has been made using both MR imaging and a computational approach. Time-resolved 3D phase-contrast MR (4D MR) [84,86,87] is an emerging technique to visualise and quantify the flow patterns in the aorta and other large arteries. Visualisation of flow patterns in the ascending aorta of a BAV patient showed strong swirling flow patterns in the ascending aorta [88]. Barker quantified ESS and demonstrated heterogenic patterns of ESS along the circumference of the ascending aorta which they implicate in asymmetric patterns of dilatation [84]. An example of computational attempts can be found in Viscardi et al. [77]. They computed ESS patterns for a different orientation of a BAV and reported that right and non-coronary cusp fusion causes higher ESS, although only one case was examined. We also made a preliminary study on a 12-year-old BAV patient (Fig. 4). This patient had a BAV without calcification, which functions well haemodynamically as seen in the smooth inflow patterns in comparison to Barker et al. However, there was hypoplasia in the aortic arch causing high blood flow velocity and subsequent highly disturbed flow downstream.

Pathological arterial wall

Involvement of structural mechanics in pathophysiological conditions of the aortic root seems to be more straightforward than that of fluid mechanics. The simplest example is tissue damage. Tissue breaks when the level of tensile stress it experiences exceeds the limit that the tissue structure can hold, i.e. its tensile strength. The reported tensile strength of human ascending/thoracic aorta shows little anisotropy and varies from 1.7 to 1.8 MPa in circumferential and 1.7 to 2.0 MPa in longitudinal directions [89,90]. Tensile strength is lower for dilated aortas (1.18 ± 0.12 MPa in circumferential and 1.21 ± 0.09 MPa in longitudinal directions) because of the loss of elastic fibres and derangements in collagen cross-linking which explains why the aneurysmal aorta has a higher possibility of rupture than the normal aorta [90]. Since the vascular wall has a layered structure, it is also important to know the inter-layer breaking strength in order to understand aortic wall dissection.

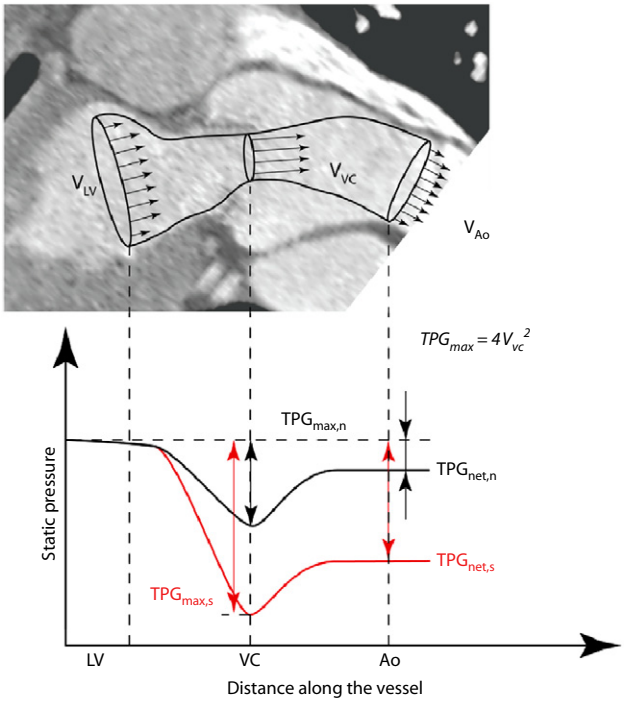

Figure. 4 **Transvalvular jet and concept of energy loss [75,81] superimposed to a longitudinal section of the aortic root from a patient who had undergone an autograft replacement operation. LV: left ventricle, VC: vena contracta, Ao: aorta, TPG: transvalvular pressure gradient. Transvalvular pressure gradient becomes higher for stenosed aortic valve (red line) than for normal valve (black line) because of a high velocity jet through the stenosed valve accompanied by turbulent flow in the downstream causing high energy loss.**

The radial strength of human aortic tissue was measured by Sommer et al. and was reported to be 140.1 ± 15.9 kPa [91], 10 times lower than the circumferential tensile strength. There are a number of computational studies aimed at understanding aneurysm rupture. Doyle and co-workers demonstrated that finite-element-based, patient-specific analysis of tensile stress can predict aneurysm rupture location as a highly concentrated stress area; rupture location was successfully predicted for 16 out of 20 cases [92]. Such computational rupture risk predictions have been attempted on abdominal aortic aneurysms [93–95] but not yet applied to thoracic aneurysm.

On the effect of stress and strain on vascular biology, an *in vitro* experiment using bovine aortic endothelium showed that cyclic strain weakly induces COX-2, suggesting up-regulated prostacyclin (PGI_2) albeit not as much as by ESS [33]. Likewise, another *in vitro* experiment on porcine valvular endothelial cells demonstrated that pro-inflammatory protein expressions were regulated by cyclic strain [34]. Up/downregulated vasoactivators and/or inflammation would alter vascular tone or stiffness, which again affects stress levels [35]. To reflect such an interaction, Rachev proposed a stress-dependent vascular remodelling rule and theoretically explained that arteries of hypertensive patients are remodelled such that the tensile stress in the wall is maintained [96]. Tissue calcifications are also associated with tensile stress [97]. In observations of excised valve tissues from surgeries, strong patterns of calcific deposits were found along the region of cusp coaptation where high stress levels are expected [98]. The potential impact of calcification was approximated by computational analyses. Hamid et al. showed that calcified sites on the aortic valve alter its dynamics and resulting vibration [99]. It was also shown, by Speelman et al., that calcification sites experienced increased tissue stress which may increase the risk of rupture [100]. This finding is supported by an *ex vivo* experimental comparison of tensile stress and strength between calcified and healthy porcine aortic walls [101]. Artificially calcified aortic tissue exhibited higher tensile stress (at 10 per cent strain, 227 ± 34 vs 147 ± 15 kPa) and lower tensile strength (1.34 ± 0.18 vs 1.55 ± 0.31 MPa) than their healthy counterparts.

As a recent example of quantifying tissue stress, Conti et al. depicted differences in tensile stress patterns in a hypothetical aortic root model with bicuspid and tricuspid aortic valves [102]. Focal high-stress regions were observed around cusp commissures, which were higher for bicuspid valves around the cusp fusion (Fig. 6). Cusp commissure is a common site of calcification [98], and the results suggest a link between elevated stress and calcification. Another computational study by Grande et al. presented stress analysis of dilated aortic roots with varying levels of dilatation [103]. Using an anatomical model based on MR images of an *ex vivo* sample, they showed elevated stress and incompetent valve coaptation for the dilated aorta, demonstrating the potential of computational method for addressing clinically relevant questions. However, patient-specific computational

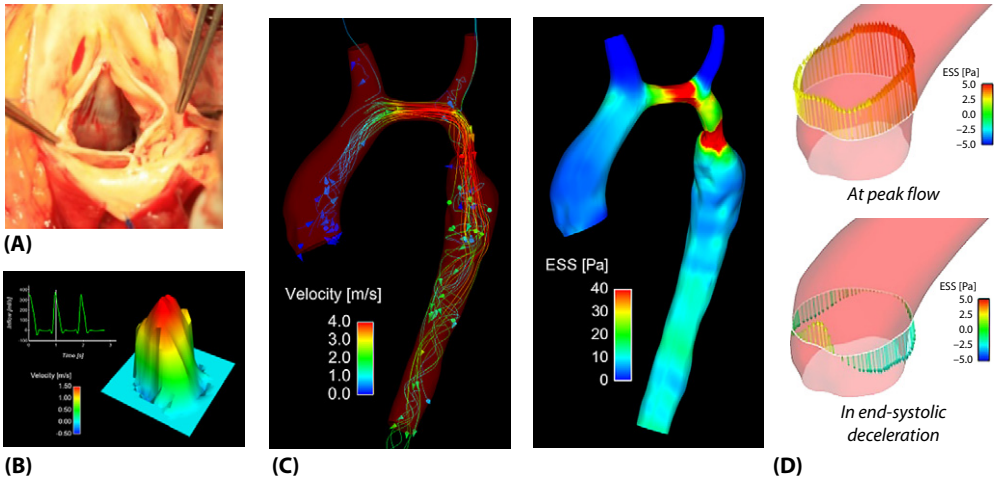

Figure. 5 **Analysis on a bicuspid aortic valve patient. (A) a photographic image taken during operation, (B) inflow profiles acquired using phase-contrast MR, (C) results from computational analysis (streamlines and endothelial shear stress map at peak flow) and (D) presentation of the ESS level along a perimeter of ascending aorta, following the method used by Barker et al. [84].**

modelling faces a number of challenges; these include geometrical modelling, estimation of material properties (constitutive relationship) and acquisition of accurate boundary conditions (reference motion), which need to rely on other imaging or *in/ex vivo* experiments. Hence it is necessary to integrate imaging, computational and other methods in order to complement each other.

Clinical interventions and their effects

Clinical interventions on the pathological aortic root can physically alter the aortic valve and root structure, resulting in changes in the biomechanical environment, e.g. structural and flow dynamics. Therefore, selection of the surgical valve substitute has a crucial impact on the short- and long-term outcomes [45].

Among the currently available aortic root substitutes, the pulmonary autograft [45,104] has been found to have a survival rate comparable to an untreated age-matched normal cohort [105]. Other stentless tissue root substitutes, e.g. homograft and porcine xenograft, are also considered effective options [106–108]. A mechanical valve is an alternative well-established choice although patients must take anticoagulants post-operatively. Each valve substitute has its specific advantages and concerns. Mechanical valves are known for good durability but, in addition to coagulation, risk of hemolysis is a matter of concern due to the high shear stress around the hinge and the regurgitant jet through the thin slit between the leaflets at valve closure [109,110]. Because of these clinical issues and relative geometric simplicity (as compared to the geometry of native valves), numerous experimental and numerical studies have been conducted on mechanical heart valves to characterise their biomechanical functions [111–113]. These works provided detailed velocity profiles at high

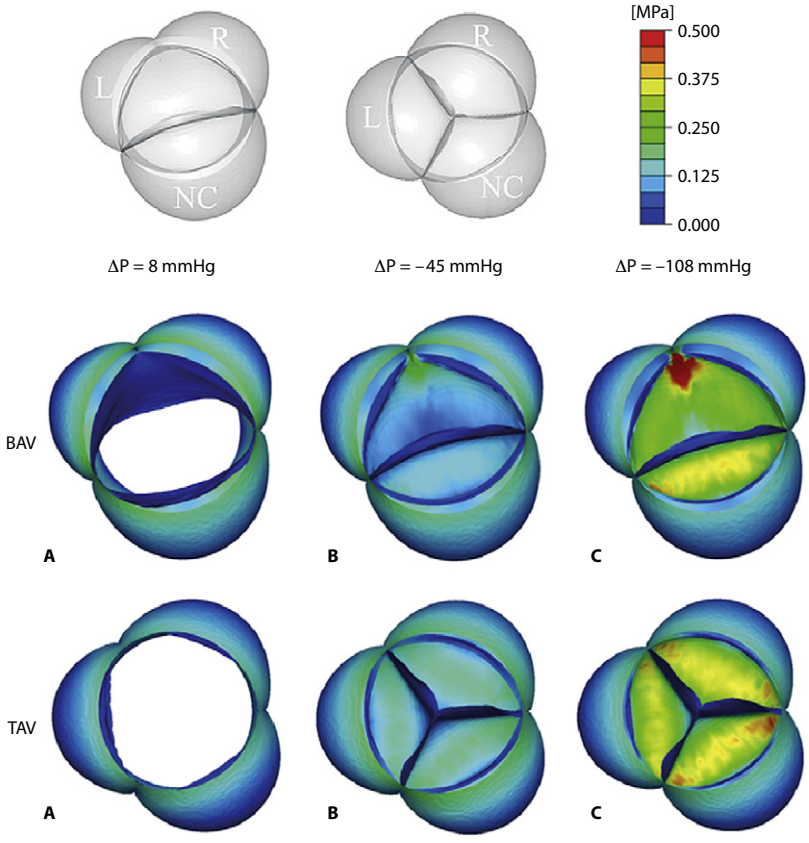

Figure. 6 Tensile stress (principal stress) distributions on aortic root and valve tissue of hypothetical aortic root models [102]. Focal high stress is observed around the leaflet commissures in closed leaflet configurations and the stress concentration is higher for the bicuspid aortic valve (BAV) model around the leaflet fusion where calcified site is typically observed [98]. Reprinted from Conti et al. J Thorac Cardiovasc Surg 140, 890–896 (2010) with permission from Elsevier.

spatial and temporal resolutions to resolve the expected highly-disturbed or turbulent flow. Initially, computations were carried out assuming a static valve with a focus on vortices behind the leaflet(s) [114]. Later, with much better computational resources, dynamic evolution of the vortices was captured with parametrically varied prosthetic designs [113]. Shear stress in the flow and on valve/arterial wall can be calculated based on such detailed flow patterns around the valve [115], which could help improve the valve design.

More favoured options, stentless tissue valves particularly with a total root replacement technique, can preserve the structural relationship between the different components of the valve mechanism and are advantageous by oversizing the annulus leading to larger orifice area [106]. Stentless tissue valves including the pulmonary autograft, homograft and xenograft (porcine bioprostheses) were reported to reproduce better haemodynamic functionality in terms of blood velocity at valvular level and transvalvular pressure gradient than mechanical valves and stented tissue valves owing to their flexibility [116–121], particularly during increased flow such as in exercise [122,123]. In particular, pulmonary autograft and porcine xenograft showed superior haemodynamic functions [117,120,123], which were suggested to contribute to their superior long-term clinical outcomes [105,106]. The flexible sinus of bioprostheses was reported to increase coronary flow [50]. Even among autograft replacements, the subcoronary grafting technique was superior to inclusion and freestanding root techniques in terms of valve dynamics, aortic flow and distensibility in an MRI-based functional evaluation study [124]. Similarly to the computational studies on mechanical valves, detailed flow characteristics resulted from the sophisticated interaction between blood flow and tissue aortic valve, and root structure could be elucidated computationally. Indeed, considerable effort has been devoted starting from Peskin and McQueen, who developed a special numerical method called immersed boundary method and applied it to a 2D heart model with valves in 1989 [125,126]. This was followed by a few other groups who developed numerical methods and demonstrated their ability to compute flow in realistic anatomical models with moving valves [127–132]. For example, Katayama and co-workers demonstrated the role of recirculating blood flow in the sinus in valve closure, by means of computational analysis of an idealised aortic root model [48].

Interestingly, the interaction between the aortic valve and blood flow is also substantially influenced by valve-sparing surgeries, even without a direct intervention on the valve itself. It has been shown that haemodynamic performance of the aortic valve after valve-sparing surgeries (sinus remodelling and valve reimplantation) are better than composite grafts in terms of TPG, particularly in exercise [133] as shown in Fig. 7A. An echocardiographic comparison of aortic valve dynamics between patients who had undergone two types of valve-sparing surgeries (tube replacement and separate replacement of the sinus of Valsalva) showed different valve opening and closing characteristics depending on the type of surgery owing to the difference in morphology and compliance of the root substitute [134,135] (Fig. 7B). An attempt to explain these findings was made later in a computational approach by Ranga et al., in which the importance of sinus reconstruction in end systolic vortex formation to help valve closure was illustrated in detail [130]. Also, a more recent MR study depicted a normalised helical flow pattern in an anatomically shaped ascending aortic graft after a Tiron David I procedure with less retrograde flow in the sinus due to altered compliance of the graft substitute [136]. These studies reinforce the importance of dynamism of the aortic root as a whole [2–7].

As far as the aortic valve is concerned, computational studies are still limited to hypothetical models aimed at understanding fundamental flow patterns and their relation to physiology, even with the most advanced computational techniques. The difficulty in computational simulation of more realistic settings lies in the difficulty in representing the complicated geometry of tissue valve leaflets. With more advanced imaging and geometrical modelling techniques, a computational approach to flow-valve interaction in more clinically-relevant settings will become possible and provide an effective tool in the near future. For example, studies with a clinical endpoint such as addressing substitute sizing issues, as performed by Matsue et al. [116], can be conducted by virtually substituting various sizes of root substitute and evaluating the haemodynamic consequences. One potential advantage computational biomechanics can offer is indeed to simulate and predict the biomechanical environment altered by surgical/intravascular/pharmacological interventions in order to assess their impact on short- and long-term clinical outcomes.

On the other hand, the influence of the valve can be incorporated in computational models by using phase-contrast MR-based velocity mapping (e.g. Suo et al. [42] and the example in Fig. 2). Such

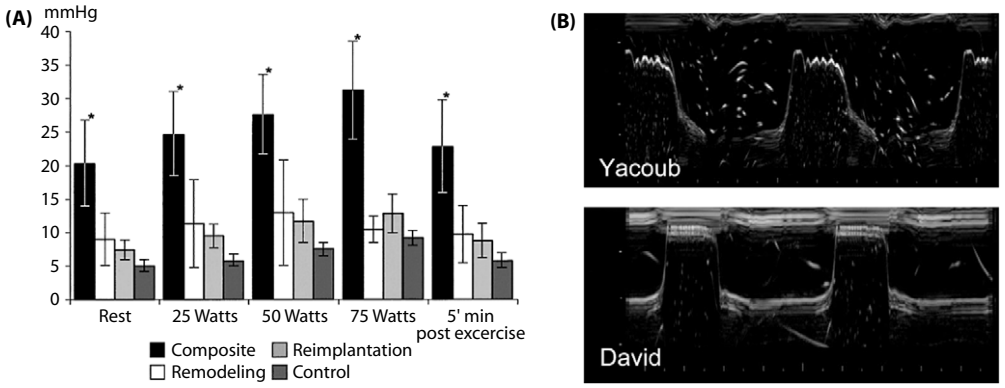

Figure. 7 Valve performance in terms of transvalvular pressure gradient (TPG) and valve dynamics. (A) A comparison of maximum TPG across the aortic valve during different levels of exercise (* significantly elevated, $p < 0.05$ [133]). An *in vivo* comparison between composite graft, aortic sinus remodelling, valve reimplantation and control showed superior performance with valve preservation techniques to composite grafts, particularly in intensive exercise. Reprinted from Graeter et al. Chest 118, 1271–1277 (2000) with permission from American College of Chest Physicians. (B) M-mode echocardiographic recordings of aortic valve motion acquired *in vitro* for remodelling (Yacoub) and reimplantation (David) techniques [135]. Even for those two techniques showed similar performance in terms of TPG showed marked difference in valve dynamics: remodelled sinus produced more gradual valve opening than valve reimplantated in a straight Dacron graft. Reprinted from Fries et al. J Thorac Cardiovasc Surg 132, 32–37 (2006) with permission from Elsevier.

an approach may be limited for the understanding of detailed flow-valve interaction but can be useful to understand flow-related events in the downstream region. Indeed, with the state-of-the-art CMR imaging technique such as one enabling the acquisition plane following the valve motion during cardiac cycle [137–139], the flow velocity mapping approach will be more accurate. Moreover, this approach is less computationally demanding. It is important to consider a balance between modelling details and computational cost, in reference to the aim of the study, demand on analysis time and available resources.

The effects of surgical intervention on aortic root structure are usually manifested through change in anatomy and mechanical properties. For example, a finite element analysis by Grande-Allen et al. showed that surgical recreation of a sinus shape reduces tensile stress in the leaflet in comparison to a cylindrical root [140,141]. Likewise, recreating sinus-like structure in the Bentall procedure reduces stress at the coronary anastomosis [142]. These are good examples demonstrating the benefits of computational modelling, allowing multiple options to be tested in patient-specific settings. Differences in mechanical properties between native tissue and root substitutes might also have a significant impact. Tensile tests of homograft, porcine xenograft and fresh porcine tissue showed similar circumferential elasticity for homograft and fresh tissue but lower elasticity (=stiffer) for the xenograft. On the other hand, the pulmonary autograft is more compliant than the aortic root [143]. As a result, the expansion of autograft in response to aortic pressure immediately after the operation was computationally predicted to be 28 per cent larger and the sinus wall was under higher tensile stress than in the pulmonary position [144]. The different biomechanical environment in the pulmonary autograft could stimulate its remodelling leading to potential autograft dilatation. However, a detailed longitudinal observation of pulmonary autograft and homograft by Carr-White and co-workers showed no significant progressive dilatation in 4 years post-operatively [145]. In the same study, homografts remained almost the same as their original size as expected from their nonviable nature. The same study additionally stated that the stress—strain relationship of their 4-month-old neoaortic root—was between that of native aorta and pulmonary artery, which indicates adaptation of neoaortic root to the new aortic environment due to its viability.

CONCLUSIONS

Over the last two decades, computational biomechanics has matured to a stage where patient-specific modelling of blood flow and wall deformation in large arteries has become a common practice. It has unique capabilities to visualise, quantify and predict biomechanical functions under conditions that mimic the *in vivo* environment. Although model assumptions are inevitable, careful

problem setup according to specific study objectives could guide one to make appropriate use of mathematical modelling tools. It is expected that further development of computational methods in conjunction with imaging techniques and biological sciences will enable computational biomechanics to address questions with clinical endpoints. More inter-disciplinary collaborations will be a key to achieve this.

ACKNOWLEDGEMENTS

Dr. Ryo Torii is a Qatar Cardiovascular Research Center Fellow supported by Qatar Foundation.

References

[1] El-Hamamsy I and Yacoub MH. Cellular and molecular mechanisms of thoracic aortic aneurysms. Nature Reviews Cardiology. 2009;6:
[2] Dagum P, Green GR and Nistal FJ et al. Deformational dynamics of the aortic root: modes and physiologic determinants. Circulation. 1999;100:II54–II62.
[3] Yacoub MH, Kilner PJ, Birks EJ and Misfeld M. The aortic outflow and root: a tale of dynamism and crosstalk. Annals of the Thoracic Surgery. 1999;68:S37–S43.
[4] Lansac E, Lim HS and Shomura Y et al. A four-dimensional study of the aortic root dynamics. Eur J Cardiothorac Surg. 2002;22:497–503.
[5] Miller DC, Cheng A and Dagum P. Aortic root dynamics and surgery: from craft to science. Philosophical Transactions of the Royal Society B-Biological Sciences. 2007;362:1407–1419.
[6] Higashidate . Regulation of the aortic valve opening: In vivo dynamic measurement of aortic valve orifice area. Journal of Thoracic and Cardiovascular Surgery. 1995;110:496–503.
[7] Lansac E, Lim HS and Shomura Y et al. Aortic root dynamics are asymmetric. J Heart Valve Dis. 2005;14:400–407.
[8] Davies JE, Parker KH, Francis DP, Hughes AD and Mayet J. What is the role of the aorta in directing coronary blood flow? Heart. 2008;94:1545–1547.
[9] Womersley JR. Method for the calculation of velocity, rate of flow and viscous drag in arteries when the pressure gradient is known. Journal of Physiology. 1955;127:553–563.
[10] Nakamura M, Wada S and Yamaguchi T. Computational analysis of blood flow in an integrated model of the left ventricle and the aorta. J Biomech Eng. 2006;128:837–843.
[11] Augst AD, Barratt DC, Hughes AD, Glor FP, Mc GTSA and Xu XY. Accuracy and reproducibility of CFD predicted wall shear stress using 3D ultrasound images. J Biomech Eng. 2003;125:218–222.
[12] Glor FP, Long Q and Hughes AD et al. Reproducibility study of magnetic resonance image-based computational fluid dynamics prediction of carotid bifurcation flow. Annals of Biomedical Engineering. 2003;31:142–151.
[13] Kung EO, Les AS, Medina F, Wicker RB, McConnell MV and Taylor CA. In vitro validation of finite-element model of AAA hemodynamics incorporating realistic outlet boundary conditions. J Biomech Eng. 2011;133:041003.
[14] Ku JP, Elkins CJ and Taylor CA. Comparison of CFD and MRI flow and velocities in an in vitro large artery bypass graft model. Ann Biomed Eng. 2005;33:257–269.
[15] Tan FPP, Torii R, Borghi A, Mohiaddin RH, Wood NB and Xu XY. Fluid–structure interaction analysis of wall stress and flow patterns in a thoracic aortic aneurysm. International Journal of Applied Mechanics. 2009;1:179–199.
[16] Ku JP, Draney MT and Arko FR et al. In vivo validation of numerical prediction of blood flow in arterial bypass grafts. Ann Biomed Eng. 2002;30:743–752.
[17] Malek AM, Alper SL and Izumo S. Hemodynamic shear stress and its role in atherosclerosis. The Journal of the American Medical Association. 1999;282:2035–2042.
[18] Cheng C, Helderman F and Tempel D et al. Large variations in absolute wall shear stress levels within one species and between species. Atherosclerosis. 2007;195:225–235.
[19] Kilner PJ, Yang GZ, Mohiaddin RH, Firmin DN and Longmore DB. Helical and retrograde secondary flow patterns in the aortic arch studied by three-directional magnetic resonance velocity mapping. Circulation. 1993;88:2235–2247.
[20] Long Q, Merrifield R, Xu XY, Kilner P, Firmin DN and G-Z Y. Subject-specific computational simulation of left ventricular flow based on magnetic resonance imaging. Proc Inst Mech Eng H. 2008;222:475–485.
[21] Faludi R, Szulik M and D'Hooge J et al. Left ventricular flow patterns in healthy subjects and patients with prosthetic mitral valves: an in vivo study using echocardiographic particle image velocimetry. J Thorac Cardiovasc Surg. 2010;139:1501–1510.
[22] Suo J, Oshinski J and Giddens DP. Effects of wall motion and compliance on flow patterns in the ascending aorta. Journal of Biomechanical Engineering. 2003;125:347–354.
[23] Morbiducci U, Ponzini R and Rizzo G et al. Mechanistic insight into the physiological relevance of helical blood flow in the human aorta: an in vivo study. Biomech Model Mechanobiol. 2011;10:339–355.
[24] Ng AC, Yiu KH and Ewe SH et al. Influence of left ventricular geometry and function on aortic annular dimensions as assessed with multi-detector row computed tomography: implications for transcatheter aortic valve implantation. Eur Heart J. 2011;
[25] Burman ED, Keegan J and Kilner PJ. Aortic root measurement by cardiovascular magnetic resonance: specification of planes and lines of measurement and corresponding normal values. Circ Cardiovasc Imaging. 2008;1:104–113.
[26] Wille SO. Numerical simulations of steady flow inside a three dimensional aortic bifurcation model. J Biomed Eng. 1984;6:49–55.

[27] Taylor TW and Yamaguchi T. Three-dimensional simulation of blood flow in an abdominal aortic aneurysm–steady and unsteady flow cases. J Biomech Eng. 1994;116:89–97.
[28] Wood NB, Weston SJ, Kilner PJ, Gosman AD and Firmin DN. Combined MR imaging and CFD simulation of flow in the human descending aorta. J Magn Reson Imaging. 2001;13:699–713.
[29] Mori D, Liu H and Yamaguchi T. Computational simulation of flow in the aortic arch - (Influence of the 3-D distortion on flows in the ordinary helix circular tube). Jsme International Journal Series C-Mechanical Systems Machine Elements and Manufacturing. 2000;43:862–866.
[30] Leuprecht A, Perktold K, Kozerke S and Boesiger P. Combined CFD and MRI study of blood flow in a human ascending aorta model. Biorheology. 2002;39:425–429.
[31] Black MM, Hose DR and Lawford PV. The origin and significance of secondary flows in the aortic arch. J Med Eng Technol. 1995;19:192–197.
[32] Shahcheraghi N, Dwyer HA, Cheer AY, Barakat AI and Rutaganira T. Unsteady and three-dimensional simulation of blood flow in the human aortic arch. J Biomech Eng. 2002;124:378–387.
[33] Kito H, Yokoyama C, Inoue H, Tanabe T, Nakajima N and Sumpio BE. Cyclooxygenase expression in bovine aortic endothelial cells exposed to cyclic strain. Endothelium. 1998;6:107–112.
[34] Metzler SA, Pregonero CA, Butcher JT, Burgess SC and Warnock JN. Cyclic strain regulates pro-inflammatory protein expression in porcine aortic valve endothelial cells. J Heart Valve Dis. 2008;17:571–577. discussion 578.
[35] El-Hamamsy I, KBalachandran K and Yacoub MH et al. Endothelium-dependent regulation of the mechanical properties of aortic valve cusps. Journal of the American College of Cardiology. 2009;53:1448–1455.
[36] Role L, Bogen D, McMahon TA and Abelmann WH. Regional variations in calculated diastolic wall stress in rat left ventricle. Am J Physiol. 1978;235:H247–H250.
[37] Cataloglu A, Clark RE and Gould PL. Stress analysis of aortic valve leaflets with smoothed geometrical data. J Biomech. 1977;10:153–158.
[38] Raghavan ML and Vorp DA. Toward a biomechanical tool to evaluate rupture potential of abdominal aortic aneurysm: identification of a finite strain constitutive model and evaluation of its applicability. J Biomech. 2000;33:475–482.
[39] Gasser TC, Ogden RW and Holzapfel GA. Hyperelastic modelling of arterial layers with distributed collagen fibre orientations. J R Soc Interface. 2006;3:15–35.
[40] Kim HJ, Vignon-Clementel IE, Coogan JS, Figueroa CA, Jansen KE and Taylor CA. Patient-specific modeling of blood flow and pressure in human coronary arteries. Ann Biomed Eng. 2010;38:3195–3209.
[41] Husmann L, Leschka S and Desbiolles L et al. Coronary artery motion and cardiac phases: dependency on heart rate — implications for CT image reconstruction. Radiology. 2007;245:567–576.
[42] Suo J, Oshinski JN and Giddens DP. Blood flow patterns in the proximal human coronary arteries: relationship to atherosclerotic plaque occurrence. Mol Cell Biomech. 2008;5:9–18.
[43] Torii R, Keegan J and Wood NB et al. The effect of dynamic vessel motion on haemodynamic parameters in the right coronary. British Journal of Radiology. 2009;82:S24–S32.
[44] Torii R, Keegan J and Wood NB et al. MR image-based geometric and hemodynamic investigation of the right coronary artery with dynamic vessel motion. Annals of Biomedical Engineering. 2010;38:2606–2620.
[45] Yacoub MH and El-Hamamsy I. The private life of tissue valves. Nature Reviews Cardiology. 2010;7:424–426.
[46] Liu X, Weale P and Reiter G et al. Breathhold time-resolved three-directional MR velocity mapping of aortic flow in patients after aortic valve-sparing surgery. Journal of Magnetic Resonance Imaging. 2009;29:569–575.
[47] Robicsek F and Thubrikar MJ. Role of sinus wall compliance in aortic leaflet function. Am J Cardiol. 1999;84:944–946. A7.
[48] Katayama S, Umetani N, Sugiura S and Hisada T. The sinus of Valsalva relieves abnormal stress on aortic valve leaflets by facilitating smooth closure. J Thorac Cardiovasc Surg. 2008;136:1528–1535. 1535 e1.
[49] de Tullio MD, Pedrizzetti G and Verzicco R. On the effect of aortic root geometry on the coronary entry-flow after a bileaflet mechanical heart valve implant: a numerical study. Acta Mechanica. 2011;216:147–163.
[50] Bakhtiary F, Schiemann M and Dzemali O et al. Stentless bioprostheses improve postoperative coronary flow more than stented prostheses after valve replacement for aortic stenosis. J Thorac Cardiovasc Surg. 2006;131:883–888.
[51] Bakhtiary F, Abolmaali N and Dzemali O et al. Impact of mechanical and biological aortic valve replacement on coronary perfusion: a prospective, randomized study. J Heart Valve Dis. 2006;15:5–11. discussion 11.
[52] Cheng C, Tampel D and van Haperen R et al. Atherosclerotic lesion size and vulnerability are determined by patterns of fluid shear stress. Circulation. 2006;113:2744–2753.
[53] Jackson MJ, Wood NB and Zhao SZ et al. Low wall shear stress predicts subsequent development of wall hypertrophy in lower limb bypass grafts. Artery Research, In press 2009;.
[54] Augst AD, Ariff B, Thom SA, Xu XY and Hughes AD et al. Analysis of complex flow and the relationship between blood pressure, wall shear stress, and intima-media thickness in the human carotid artery. American Journal of Physiology. Heart and Circulatory Physiology. 2007;293:1031–1037.
[55] Ku DN, Giddens DP, Zarins CK and Glagov S. Pulsatile flow and atherosclerosis in the human carotid bifurcation, positive correlation between plaque location and low and oscillating shear stress. Arteriosclerosis. 1985;5:293–302.
[56] Zureik M, Ducimetiere P and Touboul PJ et al. Common carotid intima-media thickness predicts occurrence of carotid atherosclerotic plaques: longitudinal results from the aging vascular study (EVA) study. Arterioscler Thromb Vasc Biol. 2000;20:1622–1629.
[57] Gijsen FJ, Mastik F and Schaar JA et al. High shear stress induces a strain increase in human coronary plaques over a 6-month period. EuroIntervention. 2011;7:121–127.
[58] Cheng C, Tempel D and van Haperen R et al. Shear stress-induced changes in atherosclerotic plaque composition are modulated by chemokines. J Clin Invest. 2007;117:616–626.

[59] Dancu MB, Berardi DE, Vanden Heuvel JP and Tarbell JM. Asynchronous shear stress and circumferential strain reduces endothelial NO synthase and Cyclooxygenase-2 but induces Endothelin-1 gene expression in endothelial cells. Arteriosclerosis, Thrombosis, and Vascular Biology. 2004;24:2088–2094.
[60] Dancu MB, Berardi DE, Vanden Heuvel JP and Tarbell JM. Atherogenic endothelial cell eNOS and ET-1 responses to asynchronous hemodynamics are mitigated by conjugated linoleic acid. Annals of Biomedical Engineering. 2007;35:1111–1119.
[61] Dancu MB and Tarbell JM. Large negative stress phase angle (SPA) attenuates nitric oxide production in bovine aortic endothelial cells. Journal of Biomechanical Engineering, Transaction of ASME. 2006;128:6.
[62] Qiu Y and Tarbell JM. Interaction between wall shear stress and circumferential strain affects endothelial cell biochemical production. Journal of Vascular Research. 2000;37:147–157.
[63] Tada S and Tarbell JM. A computational study of flow in a compliant carotid bifurcation — stress phase angle correlation with shear stress. Annals of Biomedical Engineering. 2005;33:1202–1212.
[64] Krams R, Cheng C and Helderman F et al. Shear stress is associated with markers of plaque vulnerability and MMP-9 activity. EuroIntervention. 2006;2:250–256.
[65] Vincent PE, Plata AM, Hunt AA, Weinberg PD and Sherwin SJ. Blood flow in the rabbit aortic arch and descending thoracic aorta. J R Soc Interface. 2011;
[66] Deck JD. Endothelial cell orientation on aortic valve leaflets. Cardiovasc Res. 1986;20:760–767.
[67] Gardin JM, Burn CS, Childs WJ and Henry WL. Evaluation of blood flow velocity in the ascending aorta and main pulmonary artery of normal subjects by Doppler echocardiography. Am Heart J. 1984;107:310–319.
[68] Clark C. Turbulent Velocity-Measurements in a Model of Aortic-Stenosis. Journal of Biomechanics. 1976;9:677–687.
[69] Bonow RO, Carabello BA and Chatterjee K et al. ACC/AHA 2006 guidelines for the management of patients with valvular heart disease: a report of the American College of Cardiology/American Heart Association Task Force on Practice Guidelines (writing Committee to Revise the 1998 guidelines for the management of patients with valvular heart disease) developed in collaboration with the Society of Cardiovascular Anesthesiologists endorsed by the Society for Cardiovascular Angiography and Interventions and the Society of Thoracic Surgeons. J Am Coll Cardiol. 2006;48:e1–148.
[70] Garcia D and Kadem L. What do you mean by aortic valve area: geometric orifice area, effective orifice area, or gorlin area? J Heart Valve Dis. 2006;15:601–608.
[71] Seiler C and Jenni R. Severe aortic stenosis without left ventricular hypertrophy: prevalence, predictors, and short-term follow up after aortic valve replacement. Heart. 1996;76:250–255.
[72] Chambers J. The left ventricle in aortic stenosis: evidence for the use of ACE inhibitors. Heart. 2006;92:420–423.
[73] Little SH, Chan KL and Burwash IG. Impact of blood pressure on the Doppler echocardiographic assessment of severity of aortic stenosis. Heart. 2007;93:848–855.
[74] Otto CM, Burwash IG and Legget ME et al. Prospective study of asymptomatic valvular aortic stenosis. clinical, echocardiographic, and exercise predictors of outcome. Circulation. 1997;95:2262–2270.
[75] Pibarot P and Dumesnil JG. Prosthesis-patient mismatch. Aswan Heart Centre Science & Practice Series. 2011;7:http://dx.doi.org/10.5339/ahcsps.2011.7.
[76] Briand M, Dumesnil JG and Kadem L et al. Reduced systemic arterial compliance impacts significantly on left ventricular afterload and function in aortic stenosis. Journal of the American College of Cardiology. 2005;46:291–298.
[77] Viscardi F, Vergara C and Antiga L et al. Comparative finite element model analysis of ascending aortic flow in bicuspid and tricuspid aortic valve. Artificial Organs. 2010;34:1114–1120.
[78] Bauer M, Siniawski H, Pasic M, Schaumann B and Hetzer R. Different hemodynamic stress of the ascending aorta wall in patients with bicuspid and tricuspid aortic valve. J Card Surg. 2006;21:218–220.
[79] Tadros TM, Klein MD and Shapira OM. Ascending aortic dilatation associated with bicuspid aortic valve: pathophysiology, molecular biology, and clinical implications. Circulation. 2009;119:880–890.
[80] Cheng Z, Tan FP and Riga CV et al. Analysis of flow patterns in a patient-specific aortic dissection model. J Biomech Eng. 2010;132:051007.
[81] Clark C. Energy losses in flow through stenosed valves. J Biomech. 1979;12:737–746.
[82] Fernandes SM, Khairy P, Sanders SP and Colan SD. Bicuspid aortic valve morphology and interventions in the young. J Am Coll Cardiol. 2007;49:2211–2214.
[83] Schaefer BM, Lewin MB and Stout KK et al. The bicuspid aortic valve: an integrated phenotypic classification of leaflet morphology and aortic root shape. Heart. 2008;94:1634–1638.
[84] Barker AJ, Lanning C and Shandas R. Quantification of hemodynamic wall shear stress in patients with bicuspid aortic valve using phase-contrast MRI. Annals of Biomedical Engineering. 2010;38:788–800.
[85] Barker AJ and Markl M. The role of hemodynamics in bicuspid aortic valve disease. Eur J Cardiothorac Surg. 2011;39:805–806.
[86] Markl M, Wallis W and Harloff A. Reproducibility of flow and wall shear stress analysis using flow-sensitive four-dimensional MRI. J Magn Reson Imaging. 2011;33:988–994.
[87] Markl M, Chan FP and Alley MT et al. Time-resolved three-dimensional phase-contrast MRI. J Magn Reson Imaging. 2003;17:499–506.
[88] Weigang E, Kari FA and Beyersdorf F et al. Flow-sensitive four-dimensional magnetic resonance imaging: flow patterns in ascending aortic aneurysms. Eur J Cardiothorac Surg. 2008;34:11–16.
[89] Adham M, Gournier JP and Favre JP et al. Mechanical characteristics of fresh and frozen human descending thoracic aorta. J Surg Res. 1996;64:32–34.
[90] Vorp DA, Schiro BJ, Ehrlich MP, Juvonen TS, Ergin MA and Griffith BP. Effect of aneurysm on the tensile strength and biomechanical behavior of the ascending thoracic aorta. Ann Thorac Surg. 2003;75:1210–1214.

[91] Sommer G, Gasser TC, Regitnig P, Auer M and Holzapfel GA. Dissection properties of the human aortic media: an experimental study. J Biomech Eng. 2008;130:021007.
[92] Doyle BJ, Cloonan AJ, Walsh MT, Vorp DA and McGloughlin TM. Identification of rupture locations in patient-specific abdominal aortic aneurysms using experimental and computational techniques. J Biomech. 2010;43:1408–1416.
[93] Malkawi AH, Hinchliffe RJ, Xu Y, Holt PJ, Loftus IM and Thompson MM. Patient-specific biomechanical profiling in abdominal aortic aneurysm development and rupture. J Vasc Surg. 2010;52:480–488.
[94] Maier A, Gee MW, Reeps C, Pongratz J, Eckstein HH and Wall WA. A comparison of diameter, wall stress, and rupture potential index for abdominal aortic aneurysm rupture risk prediction. Ann Biomed Eng. 2010;38:3124–3134.
[95] Vande Geest JP, Di Martino ES, Bohra A, Makaroun MS and Vorp DA. A biomechanics-based rupture potential index for abdominal aortic aneurysm risk assessment: demonstrative application. Ann N Y Acad Sci. 2006;1085:11–21.
[96] Rachev A. Theoretical study of the effect of stress-dependent remodeling on arterial geometry under hypertensive conditions. J Biomech. 1997;30:819–827.
[97] Sabbah HN, Hamid MS and Stein PD. Mechanical stresses on closed cusps of porcine bioprosthetic valves: correlation with sites of calcification. Ann Thorac Surg. 1986;42:93–96.
[98] Thubrikar MJ, Aouad J and Nolan SP. Patterns of calcific deposits in operatively excised stenotic or purely regurgitant aortic valves and their relation to mechanical stress. Am J Cardiol. 1986;58:304–308.
[99] Hamid MS, Sabbah HN and Stein PD. Vibrational analysis of bioprosthetic heart valve leaflets using numerical models: effects of leaflet stiffening, calcification, and perforation. Circ Res. 1987;61:687–694.
[100] Speelman L, Bohra A and Bosboom EM et al. Effects of wall calcifications in patient-specific wall stress analyses of abdominal aortic aneurysms. J Biomech Eng. 2007;129:105–109.
[101] Walraevens J, Willaert B, De Win G, Ranftl A, De Schutter J and Sloten JV. Correlation between compression, tensile and tearing tests on healthy and calcified aortic tissues. Medical Engineering & Physics. 2008;30:1098–1104.
[102] Conti CA, Della Corte A and Votta E et al. Biomechanical implications of the congenital bicuspid aortic valve: a finite element study of aortic root function from in vivo data. J Thorac Cardiovasc Surg. 2010;140:890–896. 896 e1–2.
[103] Grande KJ, Cochran RP, Reinhall PG and Kunzelman KS. Mechanisms of aortic valve incompetence: finite element modeling of aortic root dilatation. Ann Thorac Surg. 2000;69:1851–1857.
[104] Ross DN. Replacement of aortic and mitral valves with a pulmonary autograft. Lancet. 1967;2:956–958.
[105] El-Hamamsy I, Eryigit Z and Stevens L et al. Long-term outcomes after autograft versus homograft aortic root replacement in adults with aortic valve disease: a randomised controlled trial. Lancet. 2010;376:524–531.
[106] El-Hamamsy I, Clark L and Stevens LM et al. Late outcomes following freestyle versus homograft aortic root replacement: Results from a prospective randomized trial. Journal of the American College of Cardiology. 2010;55:368–376.
[107] Elefteriades JA. Should we abandon homografts? Journal of the American College of Cardiology. 2010;55:377–378.
[108] Wilhelmi MH. Long-term cardiac allogreaft valves after heart transplant are functionally and structurally preserved, in contrast to homografts and bioprosthesis. Journal of Heart Valve Disease. 2006;15:777–782.
[109] Travis BR, Christensen TD, Smerup M, Olsen MS, Hasenkam JM and Nygaard H. In-vivo turbulent stresses of bileaflet prosthesis leakage jets. J Heart Valve Dis. 2005;14:644–656.
[110] Dumont K, Vierendeels J, Kaminsky R, van Nooten G, Verdonck P and Bluestein D. Comparison of the hemodynamic and thrombogenic performance of two bileaflet mechanical heart valves using a CFD/FSI model. J Biomech Eng. 2007;129:558–565.
[111] Yoganathan AP, Sung HW, Woo YR and Jones M. In vitro velocity and turbulence measurements in the vicinity of three new mechanical aortic heart valve prostheses: Bjork–Shiley monostrut, omni-carbon, and duromedics. J Thorac Cardiovasc Surg. 1988;95:929–939.
[112] Walker PG and Yoganathan AP. In vitro pulsatile flow hemodynamics of five mechanical aortic heart valve prostheses. Eur J Cardiothorac Surg. 1992;6:Suppl 1, S113–S123.
[113] de Tullio MD, Pascazio G, Weltert L, De Paulis R and Verzicco R. Evaluation of prosthetic-valved devices by means of numerical simulations. Philos Transact A Math Phys Eng Sci. 2011;369:2502–2509.
[114] King MJ, Corden J, David T and Fisher J. A three-dimensional, time-dependent analysis of flow through a bileaflet mechanical heart valve: comparison of experimental and numerical results. J Biomech. 1996;29:609–618.
[115] Ge L, Dasi LP, Sotiropoulos F and Yoganathan AP. Characterization of hemodynamic forces induced by mechanical heart valves: Reynolds vs. viscous stresses. Ann Biomed Eng. 2008;36:276–297.
[116] Matsue H, Sawa Y, Matsumiya G, Matsuda H and Hamada S. Mid-term results of freestyle aortic stentless bioprosthetic valve: clinical impact of quantitative analysis of in-vivo three-dimensional flow velocity profile by magnetic resonance imaging. J Heart Valve Dis. 2005;14:630–636.
[117] Melina G, Mitchell A, Amrani M, Khaghani A and Yacoub MH. Transvalvular velocities after full aortic root replacement: results from a prospective randomized trial between the homograft and the Medtronic Freestyle bioprosthesis. J Heart Valve Dis. 2002;11:54–58. discussion 58–9.
[118] Dumesnil JG, LeBlanc MH and Cartier PC et al. Hemodynamic features of the freestyle aortic bioprosthesis compared with stented bioprosthesis. Ann Thorac Surg. 1998;66:S130–S133.
[119] Steinbruchel DA, Hasenkam JM, Nygaard H, Riis CM and Sievers HH. Blood velocity patterns after aortic valve replacement with a pulmonary autograft. Eur J Cardiothorac Surg. 1997;12:873–875.
[120] Lupinetti FM, Duncan BW, Lewin M, Dyamenahalli U and Rosenthal GL. Comparison of autograft and allograft aortic valve replacement in children. J Thorac Cardiovasc Surg. 2003;126:240–246.

[121] Jin XY, Zhang ZM, Gibson DG, Yacoub MH and Pepper JR. Effects of valve substitute on changes in left ventricular function and hypertrophy after aortic valve replacement. Ann Thorac Surg. 1996;62:683–690.
[122] Silberman S, Shaheen J and Merin O et al. Exercise hemodynamics of aortic prostheses: comparison between stentless bioprostheses and mechanical valves. Ann Thorac Surg. 2001;72:1217–1221.
[123] Porter GF, Skillington PD, Bjorksten AR, Morgan JG, Yapanis AG and Grigg LE. Exercise hemodynamic performance of the pulmonary autograft following the Ross procedure. J Heart Valve Dis. 1999;8:516–521.
[124] Luciani GB, Viscardi F, Puppini G, Faggian G and Mazzucco A. Aortic root physiology late after a "perfect" ross operation: magnetic resonance imaging study of three operative techniques. Artif Organs. 2011;
[125] Peskin CS and McQueen DM. A three-dimensional computational method for blood flow in the heart. I. Immersed elastic fibers in a viscous incompressible fluid. Journal of Computational Physics. 1989;81:372–405.
[126] Peskin CS and McQueen DM. A three-dimensional computational method for blood flow in the heart. II. contractile fibers. 1989;82:289–297.
[127] Griffith BE, Luo XY, McQueen DM and Peskin CS. Simulating the fluid dynamics of natural and prosthetic heart valves using the immersed boundary method. International Journal of Applied Mechanics. 2009;1:137–177.
[128] Weinberg EJ, Shahmirzadi D and Mofrad MR. On the multiscale modeling of heart valve biomechanics in health and disease. Biomech Model Mechanobiol. 2010;9:373–387.
[129] Shadden SC, Astorino M and Gerbeau JF. Computational analysis of an aortic valve jet with Lagrangian coherent structures. Chaos. 2010;20:
[130] Ranga A, Bouchot O, Mongrain R, Ugolini P and Cartier R. Computational simulations of the aortic valve validated by imaging data: evaluation of valve-sparing techniques. Interact Cardiovasc Thorac Surg. 2006;5:373–378.
[131] De Hart J, Peters GW, Schreurs PJ and Baaijens FP. A three-dimensional computational analysis of fluid–structure interaction in the aortic valve. J Biomech. 2003;36:103–112.
[132] De Hart J, Peters GW, Schreurs PJ and Baaijens FP. Collagen fibers reduce stresses and stabilize motion of aortic valve leaflets during systole. J Biomech. 2004;37:303–311.
[133] Graeter TP, Kindermann M, Fries R, Langer F and Schafers HJ. Comparison of aortic valve gradient during exercise after aortic valve reconstruction. Chest. 2000;118:1271–1277.
[134] Leyh RG, Schmidtke C, Sievers HH and Yacoub MH. Opening and closing characteristics of the aortic valve after different types of valve-preserving surgery. Circulation. 1999;100:2153–2160.
[135] Fries R, Graeter T and Aicher D et al. In vitro comparison of aortic valve movement after valve-preserving aortic replacement. J Thorac Cardiovasc Surg. 2006;132:32–37.
[136] Frydrychowicz A, Berger A, Stalder AF and Markl M. Preliminary results by flow-sensitive magnetic resonance imaging after Tiron David I procedure with an anatomically shaped ascending aortic graft. Interact Cardiovasc Thorac Surg. 2009;9:155–158.
[137] Roes SD, Hammer S and van der Geest RJ et al. Flow assessment throught four heart valves simultaneously using 3-dimensional 3-directional velocity-encoded magnetic resonance imaging with retrospective vavle tracking in healthy volunteers and patients with valvular regurgitation. Investigative Radiology. 2009;44:669–675.
[138] Brandts A, Bertini M and van Dijk EJ et al. Left ventricular diastolic function assessment from three-dimensional three-directional velocity-encoded MRI with retrospective valve tracking. J Magn Reson Imaging. 2011;33:312–319.
[139] Dowsey AW, Keegan J, Lerotic M, Thom SA, Firmin DA and Yang GZ. Motion-compensated MR valve imaging with COMB tag tracking and super-resolution enhancement. Medical Image Analysis. 2007;11:478–491.
[140] Grande-Allen KJ, Cochran RP, Reinhall PG and Kunzelman KS. Re-creation of sinuses is important for sparing the aortic valve: a finite element study. J Thorac Cardiovasc Surg. 2000;119:753–763.
[141] Grande-Allen KJ, Cochran RP, Reinhall PG and Kunzelman KS. Finite-element analysis of aortic valve-sparing: influence of graft shape and stiffness. IEEE Transactions on Biomedical Engineering. 2001;48:647–659.
[142] Weltert L, De Paulis R, Scaffa R, Maselli D, Bellisario A and D'Alessandro S. Re-creation of a sinuslike graft expansion in Bentall procedure reduces stress at the coronary button anastomoses: a finite element study. J Thorac Cardiovasc Surg. 2009;137:1082–1087.
[143] Matthews PB, Azadani AN and Jhun CS et al. Comparison of porcine pulmonary and aortic root material properties. Ann Thorac Surg. 2010;89:1981–1988.
[144] Matthews PB, Jhun CS and Yaung S et al. Finite element modeling of the pulmonary autograft at systemic pressure before remodeling. J Heart Valve Dis. 2011;20:45–52.
[145] Carr-White GS, Afoke A and Birks EJ et al. Aortic root characteristics of human pulmonary autografts. Circulation. 2000;102:III-15–III-21.